Indian Journal of Engineering & Materials Sciences
Vol. 30, April 2023, pp. 274-282
DOI: 10.56042/ijems.v30i2.1461

Analysis of Rotating Detonation Wave Engine

Ramanujachari V* & Amrutha Preethi P

National Centre for Combustion Research and Development, IIT Madras, Chenna 600 036, India

Received: 15 March 2022; Accepted: 31 January 2023

Rotating Detonation Wave Engine (RDE) due to its promising potential as a propulsive and power generation device has been researched worldwide based on both numerical and experimental investigations. The thermodynamic analysis has been of importance prior to the commencement of the experimental investigations as the set conditions could be established with ease. The flow field behind the detonation wave has been quite complex due to oblique shock wave, contact surface between combustion products of detonation wave and shocked combustion products and the expansion waves. The simultaneous establishment of the flow parameters has been of importance to the success of understanding the RDE. The enthalpy values at different states have provided the energy conversion to kinetic energy as a result of expansion of the product gases in the RDE flow field. Stability of the oblique shock wave attached to the detonation wave has been crucial for obtaining optimum performance of RDE. The intersection of oblique shock polar and the Prandtl – Meyer expansion characteristics has given the conditions under which the oblique shock remains attached to the detonation wave and be a part of the triple point. Under all the set conditions, the stability of the oblique shock has been ascertained. In the present analysis, the specific thrust for the present configuration using H_2–air is 1374 Ns/kg compared to a value of 1347 Ns/kg reported in the literature for a stoichiometric composition. The marginal difference has been due to the different input conditions ahead of the detonation wave. This has given credence to the results of the analytical work based on gas dynamic and thermodynamic relationships. The practical implications of this analytical work have been brought out.

Keywords: CJ detonation, Deflection angle, Rotating Detonation Wave Engine (RDE), Shock polar, Shock angle, Sonic state, Specific thrust, Specific impulse

1 Introduction

Rotating Detonation Wave Engine (RDE) would be the futuristic engine for air-breathing missile systems and gas turbine systems (aero and stationary applications). The continuous operation of RDE with an operating frequency of 3-15 kHz has been attractive for propulsion systems based on rocket, ramjet and turbojet engines. The high specific power output, thrust to weight ratio and volumetric efficiency were the characteristics of RDE based propulsion systems. Step change in thermal efficiency (by 25%) lead to less fuel consumption and emission production.[1] RDE was being evaluated for Rocketdyne's RL-10 rocket and upper stages of Delta IV and Atlas V rockets[2]. The RDE work had been carried for the first time in our country in spite of its invention in 1960[2]. The work was attempted in 3 phases. In phase-I, the RDE was designed based on the empirical correlations reported in literature[3] and the engine hardware realized[4]. In phase-II, the dynamic and thermodynamic analysis of the RDE combustor without the nozzle was carried out using the methods reported in literature[5] to obtain the realizable performance parameters. One dimensional models such as pressure history model and axial flow model were formulated and the propulsion performance parameters were computed[5]. The detailed explanation for the flow phenomena was also provided for better understanding of the complex flow. In phase-III, the ground tests were conducted in the connect pipe test facility. Expressions for thermodynamic cycles such as Brayton, Humphrey and Ficket-Jacobs (Detonation) were derived and the thermodynamic efficiencies were given for various fuels[6]. It was shown that the detonation cycle provided the maximum efficiency of about 60%. The engine performance was carried out using a zero-dimensional approach with a detailed thermochemical model of equilibrium combustion products and the specific impulse was evaluated under various injection conditions[7]. The detailed processes occurring in the RDE were very much simplified in these models. The RDE flow field could be well understood based on the two-dimensional CFD work invoking Euler unsteady equations[8, 9]. This resulted in dividing the RDE flow field into several states and models them with

*Corresponding author (E-mail: vramanujachari@yahoo.co.in)

appropriate governing equations. Similar approaches were followed by several researchers around the globe[10-14]. The power cycle calculations were coupled to non-linear dynamics of rotating detonation waves and extracted the thermodynamic metrics from particle paths in a two-dimensional unwrapped domain of RDE[15]. In order to overcome the simplifications of the reduced order models, machine learning algorithms were developed to solve the moving co-ordinate problems occurring in RDE[16]. The validation and training the software required a large amount of reliable data that is sparse. The next high fidelity model would be based on Large Eddy Simulation. As the physics of RDE was not correctly captured, these models provided over prediction of the performance parameters[17]. The major problem was the computation of the thrust and the validation. The experimental uncertainty itself was about 140% for the thrust levels less than 1000N[18].

In order to obtain the set conditions for the RDE ground tests and obtain the ballpark figures of the performance parameters, the low fidelity models including the processes occurring in various regimes of flow were selected. Initially, computations were carried out without finalizing the geometry. Later, based on the test facility capability, a particular geometry of RDE was chosen to obtain the set performance parameters. It implies that this paper focuses attention on the work carried out in phase-II of our overall plan of RDE development. NASA CEA software[19] was used to calculate the Chapman – Jouguet (CJ) detonation parameters and other thermodynamic state properties. General ideas to carry out analytical work were available in open literature[5, 10-14]. However, the detailed methodology of computations was not explicitly mentioned. Hence, the detailed methodology has been explained in this paper with a case study based on the conditions proposed for conducting the ground tests of indigenously realized RDE. Hence, there was no parametric study reported either by changing the geometry or by changing the flow input conditions. The analysis was extended further to identify the existence of the attached trailing oblique shock based on the impedance ratio of the reactants and the bounding gas ahead of the complex wave structure likely to be encountered in the proposed experiments.

2 Materials and Methods

2.1 Concept of RDE

In RDE concept, a rotating detonation wave was created using a combination of fuel and oxidizer ignited by a high intensity ignition source obtained through a pre-detonator. The combustion product gases expand through an annular nozzle producing necessary thrust. Figure 1 shows the sketch of a rotating detonation wave engine. In this case, the combustor or the detonation channel is the annular ring, where the detonation is obtained for the premixed fuel-air mixture consisting of hydrogen and air. The detonation wave propagates, near the plane of the injector circumferentially around the annular ring. The detonation products of combustion have been expanded and they flow through the exit of the combustor, which could have a nozzle to further increase the thrust. In the present case, nozzle was not considered as the scope was restricted to obtaining the rotating detonation wave under various fuel – air mixture ratios. RDE provided a continuous thrust and did not need initiation for every cycle unlike in the case of pulse detonation engine.

The study of the flow field behind the detonation wave involved analytical modeling of oblique shock wave, contact surface between combustion products of detonation wave and shocked combustion products and the expansion waves. Hence, the RDE was "unwrapped" into two dimensions[5,10-12] as shown in Fig. 2 to perform simple computations. The details are explained under "flow regimes" in this paper.

2.2 Modelling of injection process

An injection model was formulated to carry out mixing analysis of the non-premixed reactants just upstream of the detonation wave. For simplicity, one – dimensional steady flow equations of

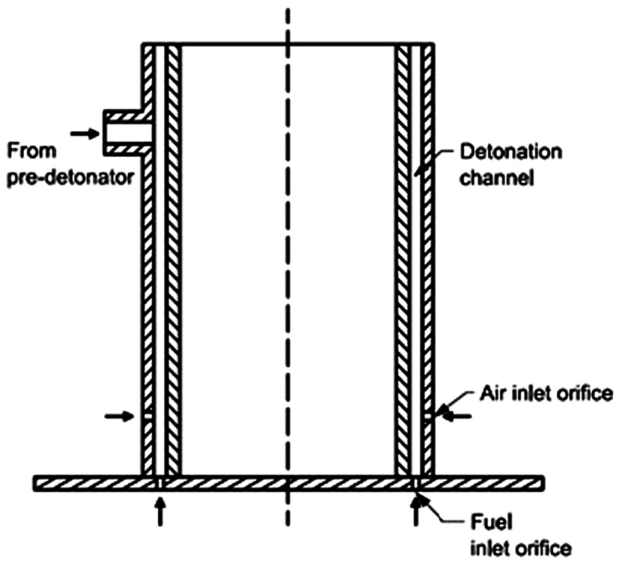

Fig. 1 — Sketch of a rotating detonation wave engine.

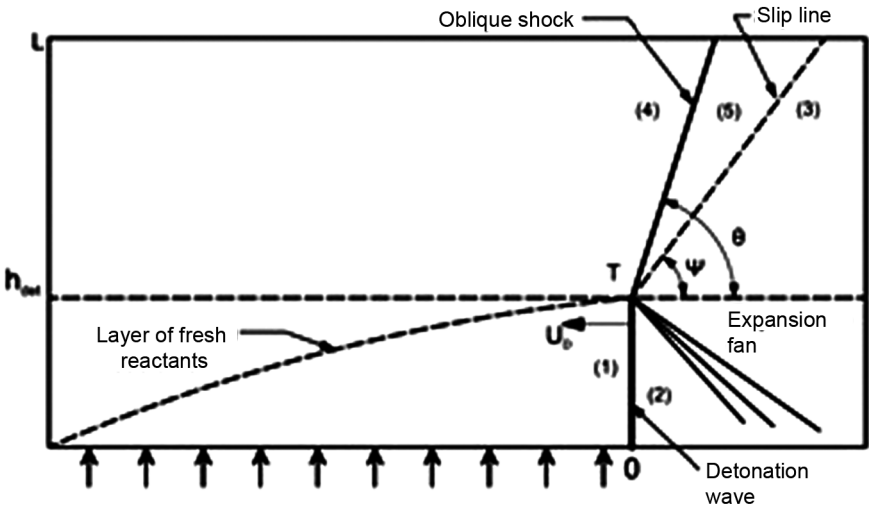

Fig. 2 — Sketch of the two-dimensional unwrapped RDE flow field.

continuity, momentum and energy were formulated and solved to obtain the mixture properties of fuel and air prior to detonation in the annular combustor based on the control volume shown in Fig. 3. State 'a' is for the air flow; state 'f' is for the fuel flow and state "mix" is for the mixture conditions. In all the cases the total pressure of the air was maintained at 3.0 bar(abs) and hence the flow rate of air was constant at 2.57 kg/s.

Depending upon the fuel based equivalence ratio the fuel flow rate was varied. As the number and diameter of the fuel injection orifices were fixed, the fuel injection total pressure was varied to allow for the required amount of fuel flow.

(a) Continuity equation

$$\dot{m}_a + \dot{m}_f = \dot{m}_{mix} \quad \ldots (1)$$

$$\dot{m}_{mix} = \varrho_{mix} A_{mix} V_{mix} \quad \ldots (2)$$

(b). Energy equation

$$\frac{\dot{m}_a}{\dot{m}_{mix}}\left(h_a + \frac{V_a^2}{2}\right) + \frac{\dot{m}_f}{\dot{m}_{mix}}\left(h_f + \frac{V_f^2}{2}\right) = c_{p,mix} T_{mix} + \frac{V_{mix}^2}{2}. \quad \ldots (3)$$

(c) Axial momentum equation

$$\dot{m}_f V_f + p_f A_f + p_a\left(A_{mix} - A_f\right) = \dot{m}_{mix} V_{mix} + p_{mix} A_{mix} \cdots \quad \ldots (4)$$

These equations were solved using Newton-Raphson method to obtain p_{mix}, T_{mix}, V_{mix}. The isentropic conditions have been invoked to obtain the stagnation pressure, stagnation temperature and Mach number at the mixture state. As the mass flow rate of air was kept constant for all the fuel based equivalence ratios, the fuel flow rate continuously increased with increase in equivalence ratio.

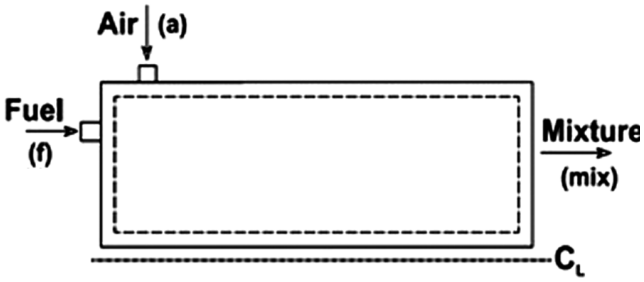

Fig. 3 — Control volume for the injection flow process.

2.3 Determination of detonation properties

NASA CEA software[19], assuming chemical equilibrium has been invoked to obtain the CJ detonation parameters such as CJ-Detonation velocity, pressure, temperature and density downstream of detonation wave. Figures 4-6 show the CJ detonation velocity, pressure and temperature as a function of fuel based equivalence ratio. The CJ detonation velocity increased with increase in equivalence ratio. This was due to the increase in sonic velocity of the gases as a result of decrease in molecular weight and increase in temperature. Heat release due to combustion also affected the CJ velocity. Heat release was appreciable as the stoichiometric condition has been approached. This in turn increased the CJ pressure and temperature as shown in Figs 5 - 6. The pressure value became almost constant in the fuel excess regime considered in this work. But, the CJ temperature decreased after attaining

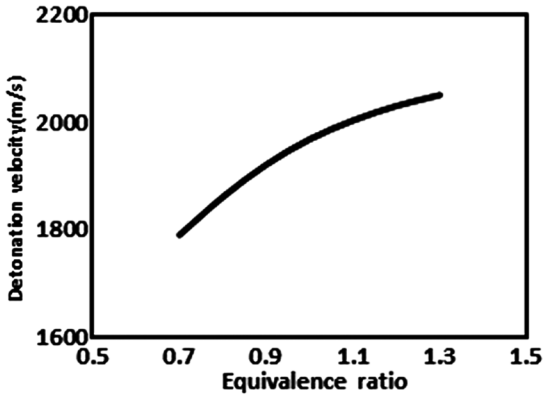

Fig. 4 — CJ Detonation velocity Vs equivalence ratio.

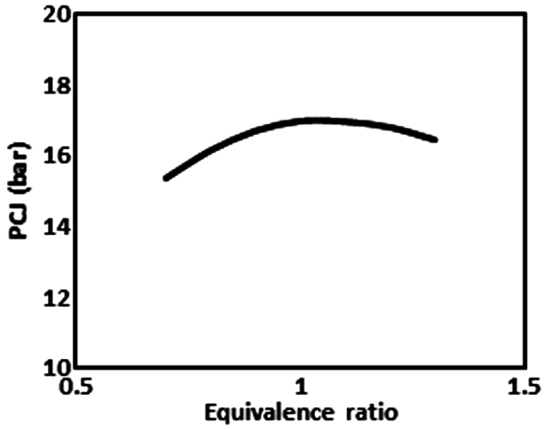

Fig. 5 — CJ Pressure Vs equivalence ratio.

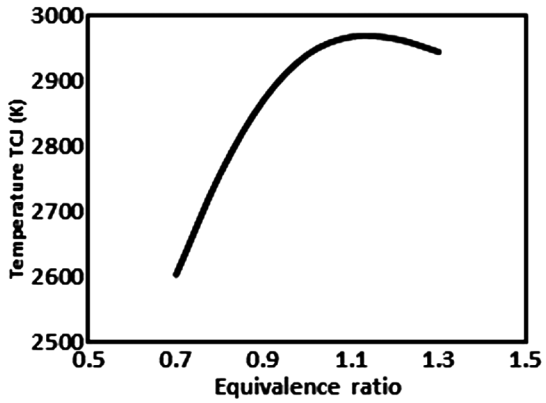

Fig. 6 — CJ Temperature Vs equivalence ratio.

maximum at stoichiometry based on chemical equilibrium computations. The stagnation enthalpy (static enthalpy at CJ condition + 0.5* square of sonic speed at CJ condition) as a function of equivalence ratio is shown in Fig. 7. It increased with equivalence ratio. This value was conserved at all the thermodynamic states considered in the flow regime of RDE at a given mixture ratio.

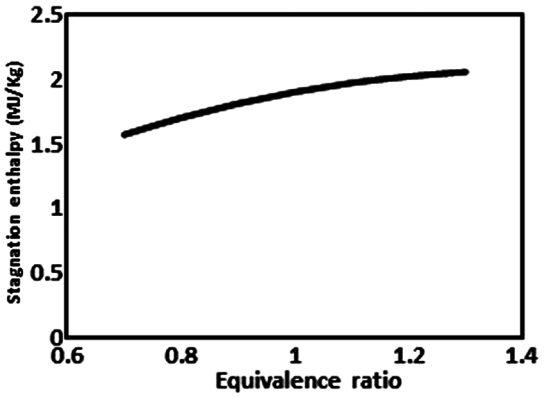

Fig. 7 — Stagnation enthalpy of the detonation products Vs equivalence ratio.

2.4 Details of flow regimes in RDE

The flow field of RDE is shown in Fig. 2. At the triple point, the detonation wave, oblique shock wave and the expansion waves meet. The slip lines start from this point. The slip line 1-4 separates the fresh reactant mixture from the products of combustion of the previous cycle of rotating detonation wave and the slip line 4-5 separated the shocked combustion products from the expanded combustion products of the detonation wave. In order to maintain mechanical equilibrium, the static pressure across the contact surfaces were assumed to be equal, which implied that $p_1 = p_4$ and $p_3 = p_5$. In the contact surface (1-4), $u_1 = u_{CJ}$ and $u_4 = u_1 + u_a$ where u_a is the azimuthal flow velocity. In this contact surface, the flow experienced a huge difference in flow velocity. The flow states of RDE were estimated based on thermodynamic analysis. The performance parameters depend on the nature of reactants, their mixture ratio, expressed in terms of fuel based equivalence ratio and the initial thermodynamic conditions such as pressure and temperature. NASA CEA computer code has been used for this purpose. The procedure of obtaining the thermodynamic states is described in this section. The input values were so chosen to obtain the plausible conditions to be set for the experiments to be conducted using the indigenously realised RDE test article.

2.5 Initial Conditions of the mixture, (State 1)

State 1 is obtained by solving the Eqs. 1-4 for the Hydrogen – Air mixture at different equivalence ratios. The values obtained for the equivalence ratio of 0.7 are given in Table 1.

2.6 Conditions downstream of detonation, (State 2)

DETN option available in NASA CEA code was utilised to calculate the conditions down stream of

detonation. Initial pressure and temperature obtained under state 1 formed the input conditions. The values obtained for the equivalence ratio of 0.7 are given in Table 2.

2.7 Conditions upstream of the oblique shock wave, (State 3)

Entropy-Pressure (S-P) option, available in NASA CEA software was utilised to obtain the state 4. It implied that the flow was isentropic between states 2 and 4. The entropy of the detonation products and the reactants at the initial pressure and temperature form the set of inputs to the code. The values obtained for the equivalence ratio of 0.7 are given in Table 3

The velocity at 4, u_4 can be calculated using H and h_4 invoking the assumption that the total enthalpy is constant. The values obtained for velocity, u_4 and Mach number at 4 were 2146 m/s and 2.69 respectively.

2.8 Downstream of expansion waves, (State 4)

Expansion of the sonic flow downstream of the detonation wave took place through Prandtl – Meyer expansion process. These waves originate from the triple point. The Mach number, static pressure and other flow properties downstream of the Prandtl – Meyer waves can be calculated with the constraint that the deflection angles and static pressures across the contact surface were equal. The governing equations are given below:

$$\tan\psi = 2\cot\theta\left[\frac{M_4^2\sin^2\theta-1}{M_4^2(\gamma_i+\cos 2\theta)+2}\right]\ldots \quad \ldots (5)$$

$$\psi = \upsilon(M_3) - \upsilon(M_2) \quad \ldots (6)$$

Table1 — Values at State 1

Static pressure, p_1	1.034 bar
Static temperature, t_1	277.4 K
Density, ϱ_1	1.024 kg/cu.m
Static Enthalpy, h_1	-30637 J/kg K
CJ Velocity, $u_1 = u_{CJ}$	1790 m/s
Sonic velocity, a_1	376 m/s

Table 2 — Values at State 2

CJ Pressure, p_{CJ}	15.36 bar
CJ Temperature, t_{CJ}	2604K
CJ Density, ϱ_{CJ}	1.819 kg/cu. m
Enthalpy at CJ state, h_{CJ}	1062500 J/kg
Entropy at CJ state, s_{CJ}	9.8 kJ/kg K
Ratio of specific heats, γ_{CJ}	1.203
Speed of sound at CJ state, a_{CJ}	1008 m/s

Table 3 — Values at State 4

Temperature at 4, t_4	1554 K
Density at 4, ϱ_4	0.2062 Kg/cu.m
Enthalpy at 4, h_4	- 731760 J/kg K
Speed of sound at 4, a_4	799 m/s.

$$\frac{P_5}{P_4} = 1 + \frac{2\gamma_i}{\gamma_i+1}(M_4^2\sin^2\theta - 1) \quad \ldots (7)$$

$$\frac{P_2}{P_3} = \left[\frac{1+[(\gamma_2-1)/2]M_3^2}{1+[(\gamma_2-1)/2]M_2^2}\right]^{\gamma_2/(\gamma_2-1)} \quad \ldots (8)$$

$$\frac{P_5}{P_4} = \left(\frac{P_1}{P_4}\right)\left(\frac{P_2}{P_1}\right)\left(\frac{P_3}{P_2}\right) \quad \ldots (9)$$

The derivations are available in the literature[10-12]. Solving the Eqs. (5-9) iteratively, the shock wave angle (θ_3), deflection angle (ψ_3), Mach number at 3 and static pressure at 3 were obtained. Using the value of pressure and invoking isentropic flow ($s_2 = s_3$), S-P (Entropy-Pressure) problem was computed by NASA CEA software to obtain the state properties at station 3. The reactants considered were at the initial temperature with a known equivalence ratio. The values obtained for the equivalence ratio of 0.7 are given in Table 4.

2.9 Conditions downstream of the oblique shock wave, (State 5)

The products of combustion flow through the oblique shock wave. The state variables at 5 were related to state variables at 4 and explained below:

Flow density downstream of the oblique shock,

$$\varrho_5 = \varrho_4 \tan(\theta_3)/\tan(\theta_3 - \psi_3) \quad \ldots (10)$$

Normal component of velocity, $u_{N4} = u_4\sin(\theta_3)$ … (11)

Enthalpy at 5,

$$h_5 = h_4 + u_{N4}^2/2 * (1 - (\varrho_4/\varrho_5)^2) \quad \ldots (12)$$

Velocity at 5, $u_5 = \sqrt{2}*(H - h_5)$; where H is the total enthalpy. The values obtained for the equivalence ratio of 0.7 are given Table 5

The enthalpy-pressure (H-P) option in NASA CEA software was used to calculate the sonic speed and

Table 4 — Values at state 3

Temperature at 3, t_3	2064 K
Density, ϱ_3	0.6222 kg/cu. M
Enthalpy, h_3	75540 J/kg K
Speed of sound, a_3	909 m/s
Shock angle, θ_3	47°
Deflection angle, ψ_3	28°
Pressure, p_3	4.15bar
Velocity, u_3	1729m/s

Table 5 — Values at State 5

Density at 5, ϱ_5	0.632 kg/cu. M
Static enthalpy at 5, h_5	375056 J/kg
Velocity at 5, u_5	1546m/s

temperature at section 5. The input to the program were pressure at 5, p_5 and enthalpy at 5, h_5 and the mixture ratio of reactants at initial temperature. The task here was to input the known quantity, h_5 to the NASA CEA program. It was not a normal procedure. For the known mixture ratio, reactant temperature was assumed and the reactant enthalpy, h_5, was calculated based on the empirical expressions of enthalpies of hydrogen and air given in the NASA CEA software. The reactant temperature was iterated till the enthalpy matches with the value obtained by Eq. 12. The output of the code gave a_5 = 941m/s and t_5 = 2235K.

2.10 Sonic axial flow state

It was reported that the flow at the exit of the RDE could be sonic[15] with the even bluff body exit (as shown in Fig. 1). But, many researchers were of the opinion that the flow at the exit was moderately supersonic (Mach number of about 1.2). The objective here was to develop a procedure for evaluating the static pressure of the axial sonic flow. In addition, the specific thrust was calculated for the hydrogen air mixture at different equivalence ratios. NASA CEA software was used to find the axial sonic flow state using the Entropy-Pressure (S-P) option keeping the entropy same as that of s_2. The NASA CEA code was used in such a way that the axial velocity obtained would be equal to sonic speed at a particular value of static pressure. The detailed procedure is given below:

The reactants at a particular mixture ratio, initial temperature, entropy s_2, arbitrary static pressures from 1.2 to 2.8 bar in steps of 0.2 bar were the input to NASA CEA software. The enthalpy of products, h_p; density of products, ϱ_p and sonic speed, a^* were obtained from the output of the program. Axial velocity was calculated from the energy conservation equation. $u_e = \sqrt{2}*(h_R - h_P)$, where, h_R is the enthalpy of reactants, that is equal to h_1 and h_P is the enthalpy of the products, that was obtained for different plausible pressures. The axial velocity and sonic velocity as a function of p/p_1 were computed and plotted in a graph. The point of intersection provided the sonic axial velocity. The corresponding value of density ϱ_P was used for the computation of specific thrust as shown below:

Specific thrust in

$$Ns/kg = u_e + (p-p_a)*1.0e05/ (\varrho_P*u_e) \quad \ldots (13)$$

Where, p_a is ambient pressure = 1 bar. The corresponding enthalpy was h_{sonic} = -0.367 MJ/kg at the equivalence ratio of 0.7. The axial velocity and specific thrust at the sonic point were 849m/s and 1172 Ns/kg respectively.

3 Results and Discussion

3.1 Pressure – Enthalpy States

The computations described in the previous section were carried out for the equivalence ratios ranging from 0.7 to 1.3. For a given reactant state 1, the enthalpy of the combustion products as a function of pressure ratio (p/p_1) is shown in Fig. 8 for the hydrogen – air mixture equivalence ratio of 0.7. This enthalpy has been a function of both pressure and entropy.

The CJ state (2) is the thermodynamic state corresponds to the highest pressure and enthalpy. There were no solutions for $p_{CJ} > p > p_m$ where, p_m was the limiting pressure corresponding to $h(p_m, s_2)$. This limiting value was 3.53 bar for the equivalence ratio of 0.7. This corresponds to the stagnation pressure (zero speed) of axial one dimensional flow. The states in between the pressure values of p_{CJ} and p_m did not have solution and hence marked in chain lines. State 4 from State 2 was arrived at based on isentropic expansion process. Here, the static enthalpy decreased drastically due to increase in the flow velocity because of the expansion of the products of detonation combustion to a pressure equal to the mixture pressure. Process 2 to 3 was the Prandtl-Meyer expansion of the products of detonation combustion. The decrease in static enthalpy was moderately low as the expansion has taken place to a higher pressure (p_3) compared to (p_4). Because of shock compression to a value p_5 which was equal to p_3 (across the slip line 3-5), the flow velocity decreased considerably from the shock upstream value leading to higher value of static enthalpy (h_5). The isentropic expansion of the detonation products was considered for the determination of the sonic state. As the static

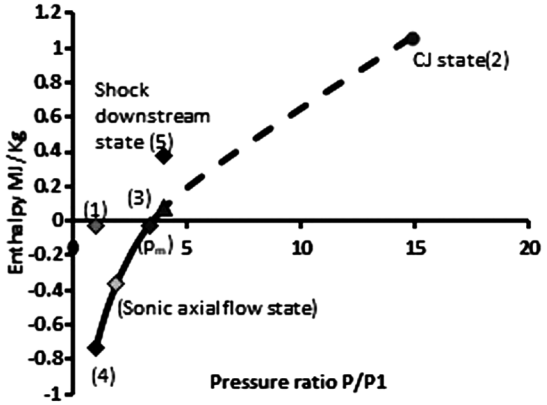

Fig. 8 — Pressure ratio Vs enthalpy at various states at equivalence ratio = 0.7.

pressure at the exit of the RDE combustor was higher than the inert gas static pressure, the expansion has taken place to a higher static enthalpy compared to that at state 4. Correspondingly, the axial flow velocity at 4 was higher than the sonic axial flow velocity. The same trend was seen for all the equivalence ratios considered in this study.

3.2 Specific thrust and specific impulse characteristics

The specific thrust is plotted as a function of the pressure ratio in Fig. 9 for the equivalence ratios of 0.7-1.3. The sonic point is indicated in this figure. Excluding the end points of pressures close to p_m and close to zero, the specific thrust is almost independent of pressure ratio and hence the value is very close to the value at sonic point for all the equivalence ratios considered in this study. The specific thrust at sonic condition as a function of equivalence ratio is shown in Fig. 10. The specific thrust reported[5] was 1374 Ns/kg which was close to the one (1347 Ns/kg) predicted in this investigation for unity equivalence ratio. The practical implication was that the specific thrust was the function of the nature of reactants, their mixture ratio, and the initial conditions and independent of the geometry of the RDE. Therefore, it is essential to understand and compute the dynamics and thermodynamics of RDE before arriving at a particular geometry of the engine.

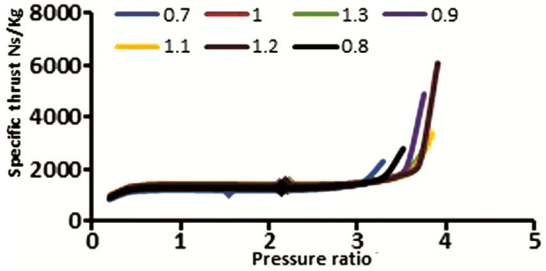

Fig. 9 — Specific thrust Vs pressure ratio at different equivalence ratios.

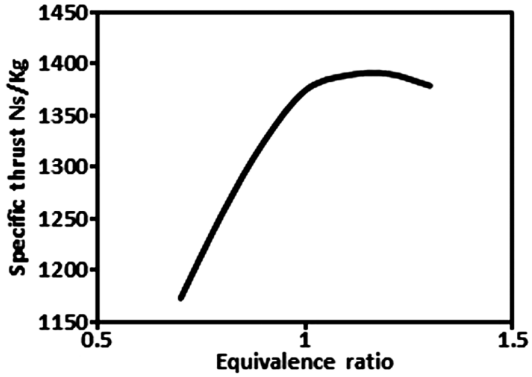

Fig. 10 — Specific thrust at sonic condition Vs equivalence ratio.

The specific impulse was derived from the specific thrust at sonic condition and mass flow rate of fuel. This depended on the geometry of the engine. The specific impulse computed was 4947s for the stoichiometric condition. It was reported[10, 20] for a wide range of area ratios (injector to combustor) and varied from 4200 to 5600 s. The value obtained in the present work is reasonably within the values reported.

3.3 Triple point characteristics

The triple point is marked "T" in Fig. 2. The implication of attached shock was that there is a solution for the shock angle, θ_3 and the deflection angle, ψ_3 by solving the Eqs. 5-9. It is evident from Fig. 11 that the shock polar intersected the Prandtl-Meyer expansion characteristics for hydrogen air mixture at an equivalence ratio of 0.7. In all the cases of equivalence ratios (0.7 to 1.3) the inert gas static temperature, t_4 varied from 1500 to 1900 K. The corresponding relative velocities at the shear layer, $(u_4 - u_1)$ were from 350 to 450 m/s. The acoustic impedance ratio ($Z_{14} = \varrho_4 a_4/\varrho_1 a_1$) values being 0.43 – 0.39. It was reported in literature[5] that the case of 3500K and velocities less than 750 m/s gave detached oblique shock solutions. This means that there was no solution to Eqs. 5-9. Houim and Fievishon[21] attributed this to the acoustic impedance ratio. Z_{14} = 0.29, corresponding to t_4 = 3500 K not giving attached oblique shock solution. The practical implication was that the arbitrary changes to t_4 and u_4 need not be done to see the possibility of the attached oblique shock. Instead, realistic cases will have to be considered to know the behaviour of the oblique shock.

Shepherd and Kasahara[5] opined that the existence of the attached oblique shocks depended on the ratio of specific heats and Mach number at condition 1 and 4 and not on Z_{14} alone. As the state point 4 is uniquely

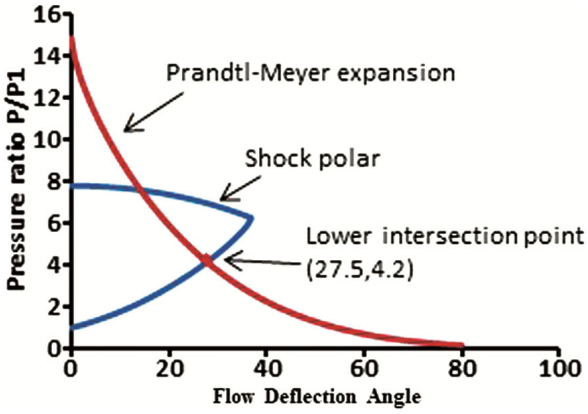

Fig. 11 — Flow deflection angle Vs pressure ratio at equivalence ratio = 0.7.

fixed for a given condition at state point 1, based on the simple thermodynamic model, the phenomenon of the attached oblique shock seemed to depend on the initial conditions only. More investigations are required in this area to get an insight into this phenomenon. The present theoretical investigation indicates that the detached oblique shock will not be seen in the experimental conditions to be set and hence the initial design of RDE can be carried out with the assumption of stable attached oblique shock. Experimental investigation involving huge set of conditions may reveal the criterion for existence or non-existence of the stable attached oblique shock, which will be done in the next phase of study.

4 Conclusion

The conclusions of this study are as follows:

- The specific thrust has been independent of the hardware configuration and depends on the fuel – oxidizer mixture and initial conditions ahead of the detonation wave. For a given initial condition, reactants and their composition, the specific thrust has been independent of the combustor exit pressure. Hence, specific thrust has been considered for propulsion performance computations from the sonic flow analysis. These characteristics have been of practical relevance as the computations could precede the hardware realisation. Also, the hardware geometry could be arrived at based on the flow capabilities of the test facility. The specific thrust resulted from the present analysis for our requirement of using H_2 –air at stoichiometric mixture is 1374 Ns/kg compared to a value of 1347 Ns/kg reported in literature. These are the reasonable matching values given certain improvements made in the present study such as incorporation of the two-stream mixing model.
- The Pressure – Enthalpy plot has provided the amount of kinetic energy converted from the total enthalpy in various flow regimes. This has been ultimately used in the computation of propulsion parameters at the combustor exit. The equivalent stagnation pressure in rocketry could be obtained by considering the kinetic energy to be zero. All the states from 1 to 5 are having equal stagnation enthalpies. As this analysis has been independent of the injection system, the velocity of injection had been neglected compared to the CJ detonation velocity in the calculation of stagnation enthalpy under Moving Frame coordinate system.
- The flow deflection analysis has provided the conditions under which the trailing oblique shock attaches to the triple point of RDE. The slip line angle (deflection angle) was obtained by ensuring the oblique shock attachment using the intersection of shock polar with the Prandtl Meyer expansion wave characteristic. They will not intersect if the shock is detached. Most of the realistic experimental operating conditions of RDE ensure the stability of the trailing oblique shock wave. This has been achieved due to the higher acoustic speed, and hence the higher static temperature of the products of combustion ahead of the trailing oblique shock, leading to higher acoustic impedance ratio. The acoustic impedance along the contact surfaces (between 1 & 4 and between 3 & 5) and the differential velocity ($u_4 – u_1$) could be derived from this model to evolve a criterion for the attached oblique shock. Thus, the shock stability cases have to be identified before performing the experiments.
- Axial sonic flow analysis has provided the value of specific thrust. From that, we can get the specific impulse for a given geometry of the engine and the corresponding detonation parameters.
- The specific impulse computed in the present study for H_2 – Air at stoichiometry was 4947s. A range of values of 4200 – 5600s was reported in open literature.
- After obtaining the experimental data, the short comings or strength of these simple models have been assessed and corrective actions have been taken using high fidelity models based on CFD.

Acknowledgement

CSIR, Government of India is acknowledged for sanctioning the research funds to the senior author under the CSIR Bhatnagar Fellowship award. The authors thank Prof. S R Chakravarthy, Coordinator, NCCRD, IIT, Madras for the research and administrative support.

References

1 Journell C L, *High speed diagnostics in a natural gas-air rotating detonation wave engine at elevated pressure*, PhD thesis, Purdue University, 2019

2 Sooraj Ram, *The impossible RDE actually works,* Advancetec News, 26 May 2020

3 Subramaniam S, *Novel approach for computational modelling of a non-premixed rotating detonation wave engine*, MS thesis, Virginia Polytechnic Institute and State University, 2019

4 Ramanujachari V & Preethi A P, Transactions of the Indian National Academy of Engineering, 2021. https://doi.org/10.1007/s41403-021-00275-2.

5 Shepherd J E & Kasahara J, *Analytical models for the thrust of a rotating detonation engine*, GALCIT Report, CIT, CA, USA, 2017

6 Shah I J, Kildare J AC, Ivans M J, Cinnici A, Sparks C A M, Rubaiyat S N H Cin R C & Medwell P R, *Detonation – A new era for Engines,* Intech Open, 2019

7 Fotia M L, Hoka J & Schauer F, *Performance of rotating detonation wave engine for air breathing applications*, Chapter.1, in *Detonation Control for Propulsion, Shock Waves and High Pressure Phenomena*, Edited by Li, J.M. (Springer, 2018,Singapore)https://doi.org/10.1007/978-3-319-689067_1, (2018)

8 Escobar S, Suryanarayana RP, Ismail C, Donald Ferguson & Peter Strakey, Proceedings of ASME Turbo Expo, GT2013-94918, (2013).

9 Schwer, D & Kailasanath, K, 51st AIAA/ SAE/ASEE Joint Propulsion Conference, AIAA 2015-3782, 2015.

10 Sousa J, Braun J & Paniagua G, Applied Math Modelling, Vol 52 (2017) 42.

11 Fievisohn R, *Development and Application of Theoretical Models for Rotating Detonation Wave Engines*, PhD thesis, University of Maryland, USA, 2016

12 Mizener A R, *Performance Modelling and Experimental Investigations of Rotating Detonation Engines*, PhD thesis, University of Texas at Arlington, USA, 2018

13 Lu F K & Braun E M, Journal of Propulsion and Power, 30 (2014) 1125.

14 Han H S, Lee E S & Choi J Y, Energies,14,Paper-1381,2021

15 Koch J & Kutz N, Physics Fluids, 32(2020), 126102(1- 20).

16 Mendible A, Koch J, Lange H, Bruntor S L & Kutz N, Phys. Rev. Fluids, Paper 050507,6 (2021)

17 Bennewitz J W, Bigler B R, Hargus W A & Smith RD, Energies,14, Paper- 2037, 2021.

18 Suchocki J A, *Operational space and characterisation of a rotating detonation engine using hydrogen and air*, MS thesis, The Ohio State University, USA, 2012

19 Gordon S & McBride B, *NASA Chemical Analysis Equilibrium Code*, NASA Glenn Centre, 1996

20 Schwer D A & Kailasanath K, AIAA paper 2011-0581, 2011

21 Houim R W & Fievishon R T, Combustion & Flame, 179 (2017) 185